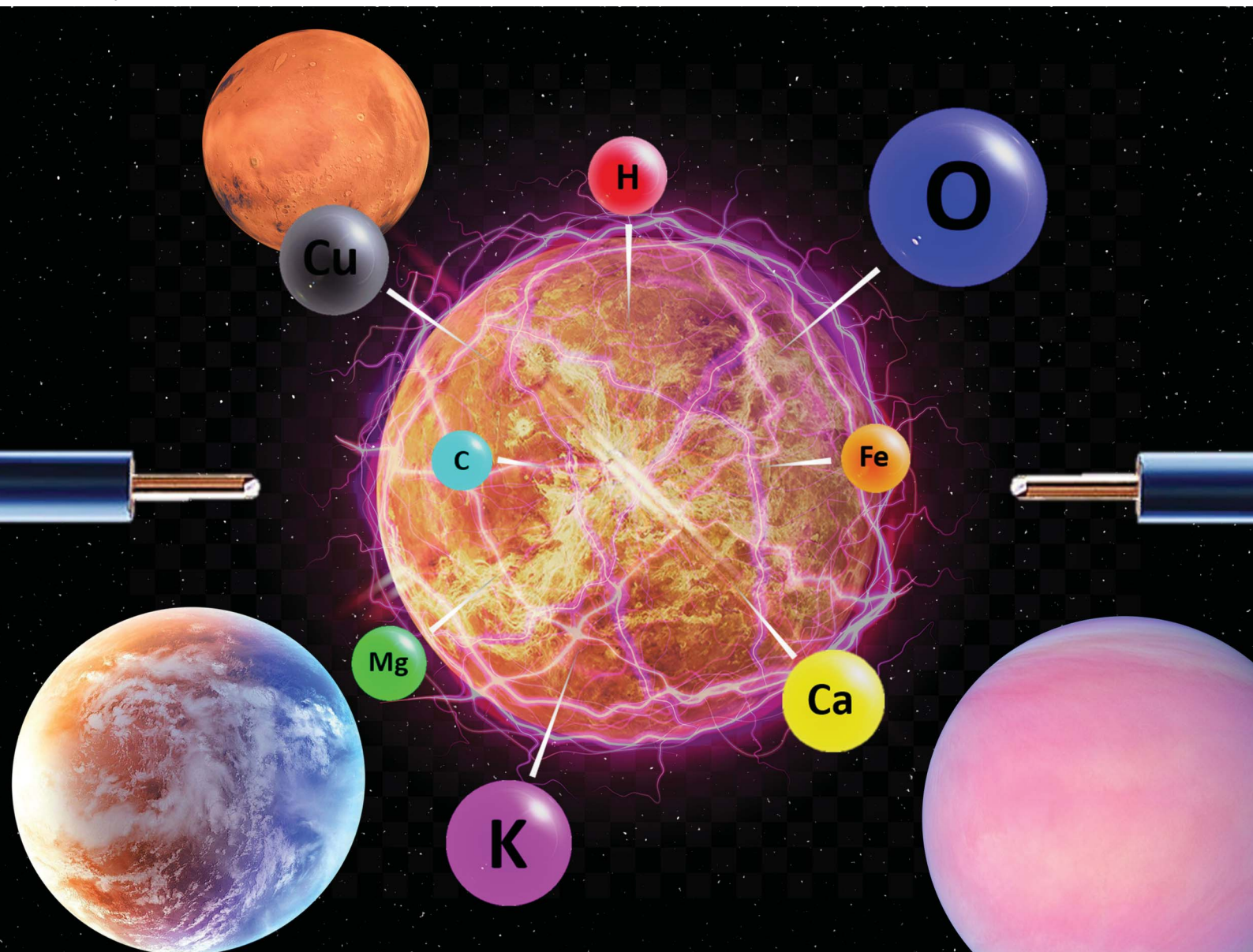


JAAAS

Journal of Analytical Atomic Spectrometry

rsc.li/jaas



ISSN 0267-9477

PAPER

Jack J. Yoh *et al.*

An optimal configuration for spark-induced breakdown spectroscopy of bulk minerals aimed at planetary analysis

PAPER



Cite this: *J. Anal. At. Spectrom.*, 2020, 35, 1103

An optimal configuration for spark-induced breakdown spectroscopy of bulk minerals aimed at planetary analysis

Jaehun Jung,^a Jun-Ho Yang^b and Jack J. Yoh *^b

Spark-induced breakdown spectroscopy (SIBS) utilizes an electric spark to induce a strong plasma for collecting atomic emissions. The spark is an electric discharge characterized by a high voltage and low current, which occurs when the applied voltage between electrodes is higher than the breakdown voltage of the ambient surroundings of the electrodes. This study analyses the potential for using a compact SIBS instead of conventional laser-induced breakdown spectroscopy (LIBS) in discriminating rocks and soils for planetary missions. Targeting bulky solids using SIBS has not been successful in the past, and therefore a series of optimizations of electrode positioning and electrode materials were performed in this work. The limit of detection (LOD) was enhanced up to four times compared to when LIBS was used, showing a change from 78 to 20 ppm from LIBS to SIBS. Within the same CCD gate delay time and width, the signal intensity for SIBS was substantially higher than for LIBS by three orders of magnitude, due to the higher energy of plasma generated. Changing the electrode material and locating the optimum position of the electrodes were considered for optimizing the current SIBS setup being tested for samples of planetary origin.

Received 15th February 2020
Accepted 24th March 2020

DOI: 10.1039/d0ja00057d

rsc.li/jaas

1. Introduction

Scientists have investigated the constituent materials of unknown samples acquired from manned or unmanned exploratory missions. Compared to the virtuous environment on Earth, the outer planets feature conditions that can be both extreme and unpredictable. Emission spectroscopy is an effective analytical method that can remotely detect, identify, measure, and monitor rock samples of remote sites. It also provides access to various types of information, such as the molecular composition, atmospheric conditions and motion of an object, that can be obtained by remotely sensing spectral emissions. Thus, emission spectroscopy can play an important role in interpreting the space environment for the safety and effectiveness of future discovery missions.

Laser-induced breakdown spectroscopy (LIBS) has been shown to be quite promising for space missions.¹ LIBS is an atomic emission spectroscopic method that captures the specific spectra emitted from the surface excitation of the target sample. In recent decades, LIBS combined with Raman spectroscopy has been the focus of research into providing an on-board, *in situ*, real-time, and multi-elemental measurement technology.^{1–3}

However, the cost and poor sustainability of the pulse laser system in an extreme environment limit the general utilization of LIBS in wider applications. As an alternative, spark-induced, as opposed to laser-induced, breakdown spectroscopy is considered to be a replacement technique to supplement the known weaknesses of the available atomic spectroscopies. SIBS uses the plasma formed by the strong electric field as breakdown occurs, and the material between the electrodes is ionized and becomes conductive. Following the atomic emission spectroscopic principle, the characteristic emission lines are collected, and the emission peaks are analyzed to identify the species present. Despite its compact size and the fewer components required than in a comparative optical spectroscopic setup, the spark has a considerably larger volume, of the order of 0.07 cm³, than the typical laser-induced plasma volume of 0.003 cm³ from a single-pulse 100 mJ Nd:YAG laser.⁴

Notwithstanding the substantial advantages of SIBS, the research venturing into this area is quite minuscule compared to that on LIBS. In recent research by Letty *et al.*,⁵ SIBS has been proven to offer an improved signal-to-noise ratio for the determination of fuel concentration, although LIBS offers higher accuracy due to lower background emissions. A comparison of LIBS and SIBS was also carried out for the measurement of airborne particulates and heavy metal contamination in soils.⁶ Kammermann *et al.*⁷ also used SIBS to obtain the fuel–air equivalence ratio and the hydrogen-enrichment level of methane analysis in modern-day bivalent engine research. In,⁸ the determination of mercury in soils was performed in

^aDepartment of Aerospace System Engineering, Seoul National University, Republic of Korea

^bDepartment of Mechanical and Aerospace Engineering, Seoul National University, 1 Gwanakro, Gwanakgu, Seoul, 08826, Republic of Korea. E-mail: jjyoh@snu.ac.kr

a comparison. It turned out that LIBS reached its optimum activity at higher concentrations, while SIBS performed better at lower mercury concentrations.

A combined method called spark-assisted laser breakdown spectroscopy (SA-LIBS) to enhance analytical sensitivity and the limit of detection in industrial applications has been outlined.^{9,10} Even though LIBS has been widely applied to the elemental analysis of multiple industrial fields, there are some known drawbacks, such as matrix effects due to the complex nature of the plasma-particle interactions followed by the low analytical sensitivity and signal due to the low excitation efficiency of the atoms in the excitation process. Also, the influence of a strong continuum background in the laser-induced plasma is another known drawback.¹¹ SA-LIBS is one approach to improving the analytical sensitivity of LIBS, such as double-pulse excitation,¹² spatial confinement,¹³ magnetic confinement,¹⁴ and glow discharge excitation.¹⁵ The limit of detection of lead and aluminum was improved by three times going from LIBS to SA-LIBS.¹⁶

The weakness of SIBS is the difficulty in manually positioning the electrical spark onto a bulk sample. The lack of physical contact disturbs the formation of the electric fields required for the breakdown of the sample surface. Also, it can hardly be adopted for non-conducting samples unless it creates a plasma strong enough that the plasma ball can lead to erosion of the sample.¹⁷ These weaknesses of SIBS call for research into optimising the electrodes in the solid-phase breakdown. To optimise the SIBS setup for solid-phase breakdown, various experiments have been tried, such as changing the electrode shape and materials, and setting up different distances between the two electrodes. Additionally, spark-induced emission spectra were also tested across the electrode gap with methane/air and hydrogen-enriched methane/air mixtures.⁷ The results showed that the emission lines of OH, NH, CN and N₂ were not distributed equally across the electrode gap, suggesting that further studies should be conducted to determine the cause of this variation.

The objectives of this work are (i) to characterize the plasma based on the atomic emission lines, (ii) to perform advanced SIBS in targeting bulk material samples of possible planetary origin, which has never been done previously, (iii) to compare SIBS and LIBS within the scope of signal sensitivity and strength, (iv) to devise an optimised SIBS device by spatially resolving the emission spectra across varying electrode positions and materials, and (v) to investigate the potential for using SIBS in an extreme space environment.

2. Materials and methods

2.1 Sample preparation

2.1.1 Preparation of rock samples. A total of sixteen pure rock samples were analyzed without any chemical preprocessing, as listed in Table 1. Those rock minerals were chosen for this study, due to their high possibility of existence on Mars but which are also available on Earth.^{18,19} The size of each rock sample was approximately 4 cm × 4 cm × 4 cm, and each rock composition was known to be pure. Most preceding SIBS

studies have used powder or pellet samples in their solid material analysis.^{20,21} In,²² it was shown that the relative standard deviations (RSDs) from using pellet samples in SIBS were smaller than those from other sample forms, such as particle and bulk shapes. However, in this study, pure bulk-shaped samples were used for both SIBS and LIBS for further studies in order to build SIBS systems in a practical environmental application. Table 2 compares the target sample setups in the SIBS studies. An explanation of each type is given in Section 2.2.2.

2.1.2 Preparation of pellet samples. Aragonite (CaCO₃) powder in pellet form was used for the calibration curve and stand-off tests discussed in Sections 3.2 and 3.3. A paraffin binder (SPEX sample Prep., 3646–450), which is in an inactive phase during the plasma ablation, was mixed with aragonite powder to present the relationship between the concentration of a chemical substance and signal intensity for the calibration curve. In addition, the paraffin binder is made up of carbon and hydrogen (C_nH_{2n+2}) and blends quickly and completely with the samples. A SPEX model 3635 was used to pelletize the mixed powder with 10 tonnes of pressure for 2.5 min of dwell time and 1.5 min of release time. The quantities of the powder sample and paraffin binder were 3.0 mg and 3.0 g, respectively.

2.2 Instrumentation and operation

2.2.1 Experimental setup. A customized SIBS system was assembled for this experiment. Two pure tungsten cylindrical rods of 1.0 mm diameter were mounted on sample holders which were built to perform flexible adjustment of the electrode separation and the position of the electrode tips. The electrodes were placed ~3 mm apart. A high-voltage DC module (UltraVolt 6C24-P30, 6 kV, 90 mA), and high-voltage capacitors (HVCAP DMS HV Capacitor, 0.1 μF, 30 000 Vdc) were built in a compact SIBS device sized at 15 cm × 15 cm × 4 cm. The customized compact device was composed of those high-voltage spark installations, an AC–DC converter, and a micro control unit (Arduino BLE) replacing the pulse generator for three specific functions; voltage intensity, spark discharge time, and trigger signal. A simple schematic of the SIBS and LIBS experimental setup is shown in Fig. 1. To compare the analytical results for SIBS, an LIBS experiment was built with a Q-switched Nd:YAG laser (Surelite II, Continuum Inc.) and an RT-250Ec-CCD Camera (Applied Spectra Inc.). In both spectroscopic methods, the plasma signals were captured by an optical fiber placed alongside the two electrodes and transmitted to a spectrometer (Michelle 5000, Andor) coupled with an ICCD camera (iStar, Andor) and the six-channel CCD cameras (RT250-Ec, Applied Spectra Inc.) to detect the plasma in the wavelength range of 198–1050 nm. The gate width of the ICCD and CCD was fixed at 1 ms, and the delay time was set to 1 μs for both methods. For each sample, an average of 100 shots were fired onto its surface for both the SIBS and LIBS experiments. It was found that the SIBS ablation rate was approximately constant for the first 20 spark shots, with the crater depth being about 0.3 mm, while for LIBS it was 100 shots and 0.09 mm. Due to the effect of the ablation crater on the signal intensity, the positions

Table 1 Chemical information and representative peaks of mineral samples

Samples	Molecular information	Atomic information
Aragonite	CaCO ₃	Ca (393.37, 396.85, 422.67, 646.26 nm), C (283.67, 283.76 nm), O (777.298 nm)
Azurite	Cu ₃ (CO ₃) ₂ (OH) ₂	Cu (219.22, 324.754, 327.396 nm), C (283.67, 283.76 nm), O (777.298 nm), H (656.3 nm)
Barite	BaSO ₄	Ba (455.403, 553.548 nm), S (545.38, 543.28, 757.89, 762.97, 831.46 nm), O (777.298 nm)
Copper	Cu	Cu (219.22, 324.754, 327.396 nm)
Dolomite	CaMg(CO ₃) ₂	Ca (393.37, 396.85, 422.67, 646.26 nm), Mg (285.213, 279.55 nm), C (283.67, 283.76 nm), O (777.298 nm)
Emerald	Be ₃ Al ₂ Si ₆ O ₁₈	Be (234.86, 313.04, 313.10 nm), Al (281.61, 396.15, 466.30 nm), Si (221.09, 221.67, 251.61, 288.159 nm), O (777.298 nm)
Fusion silicone	Si(SiO ₂)	Si (221.09, 221.67, 251.61, 288.159 nm), O (777.298 nm)
Graphite	C	C (283.67, 283.76 nm)
Gypsum crystal	CaSO ₄ ·2H ₂ O	Ca (393.37, 396.85, 422.67, 646.26 nm), S (545.38, 543.28, 757.89, 762.97, 831.46 nm), O (777.298 nm), H (656.3 nm)
Halite	NaCl	Na (309.27, 328.56, 588.99, 589.59 nm), Cl (479.45, 489.67, 542.32 nm)
Hornblende	(Ca, Na) ₂ -3(Mg, FeAl) ₅ (Al, Si) ₆	Ca (393.37, 396.85, 422.67, 646.26 nm), Na (309.27, 328.56, 588.99, 589.59 nm), Mg (285.213, 279.55 nm), Fe (238.2, 239.56, 248.32 nm), Al (281.61, 396.15, 466.30 nm), Si (221.09, 221.67, 251.61, 288.159 nm)
Olivine	(Mg, Fe) ₂ SiO ₄	Mg (285.213, 279.55 nm), Fe (238.2, 239.56, 248.32 nm), Si (221.09, 221.67, 251.61, 288.159 nm), O (777.298 nm)
Pyrite	FeS ₂	Fe (238.2, 239.56, 248.32 nm), S (545.38, 543.28, 757.89, 762.97, 831.46 nm)
Sulfur	S	S (545.38, 543.28, 757.89, 762.97, 831.46 nm)
Talc	Mg ₃ Si ₄ O ₁₀ (OH) ₂	Mg (285.213, 279.55 nm), Si (221.09, 221.67, 251.61, 288.159 nm), O (777.298 nm), H (656.3 nm)
Vanadinite	Pb ₅ (VO ₄) ₃ Cl	Pb (220.35, 280.19, 405.78 nm), V (290.88, 292.40, 309.31, 310.22, 311.07 nm), O (777.298 nm), Cl (479.45, 489.67, 542.32 nm)

of the ablation focus were shifted by millimeters every 10 shots for SIBS and 0.1 millimeters every 30 shots for LIBS. To average the signal data for both experiments, outlier data were excluded from every calculation. In addition, a specific 30 accumulation

spectrum from a calcite sample was collected for the purpose of a calibration curve.

2.2.2 Compact-sized SIBS setup. As briefly mentioned in Section 2.2.1, a customized compact SIBS setup was used for

Table 2 Comparison of samples and setup in the SIBS analysis^a

Experimental setup	Target sample/size	Reference
Spark plug (Type I)	Methane/air mixtures (aerosol)	Kammermann <i>et al.</i> ⁷
Spark plug (Type I)	Airborne particulates and solid samples/powder	Hunter <i>et al.</i> ⁴
SIBS (Type II)	Soil/powder	Strungaram <i>et al.</i> ⁸
SIBS (Type II)	Particles with different carbon contents/powder	Yao <i>et al.</i> ²⁰
SIBS (Type II)	Cement/powder	Taefi <i>et al.</i> ²¹
SA-SIBS (Type III)	Metals/small-sized scrap	Liu <i>et al.</i> ²³
SIBS (Type IV)	16 pure rock minerals/bulk material – practical size	Present setup

^a Type I uses a spark plug originally used in car engines. This is frequently used for testing the gaseous phase in SIBS research. Type II replaces the spark plug of Type I with two long electrodes to optimize the positioning of the sparks on the sample surface. Type III is SA-LIBS that implements both SIBS and LIBS (laser-induced breakdown spectroscopy). Type IV is a compact SIBS with a size of 15 cm × 15 cm × 4 cm, where the pulse generator of Type II is replaced by a micro control unit for controlling the size and frequency of the plasma.

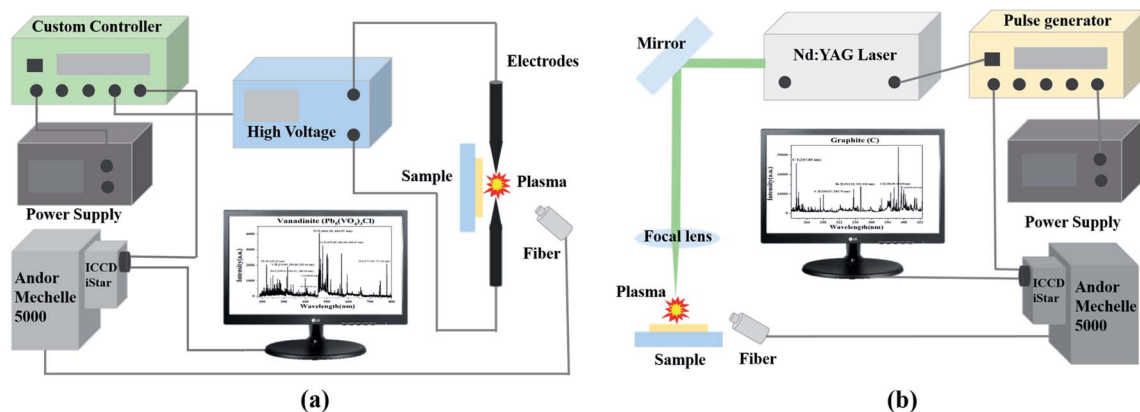


Fig. 1 Simple schematics for (a) compact SIBS and (b) conventional LIBS.

this experiment. There are three reported types of SIBS, as seen in Table 2. Type I uses a spark plug originally used in car engines. This is frequently used for testing the gaseous phase in SIBS research. Type II replaces the spark plug with two long electrodes to optimize the positioning of the sparks on the sample surface. Type III is an SA-LIBS that implements both SIBS and LIBS. Type IV is the present SIBS setup, where its compactness stands out, with its size being $15\text{ cm} \times 15\text{ cm} \times 4\text{ cm}$. The conventional pulse generator is replaced by the compact micro control unit which controls the size and frequency of the plasma and is compatible with the ICCD system. Fig. 2 illustrates how to control the gate on-off of the ICCD camera using the MCU by sending an electrical signal after the capacitor charging time has passed. In addition, a wireless-type MCU was chosen to replace wire adaptors between the computer and the SIBS controller. In order to save space, the components were made compact. Relatively, this proves to be a major advantage in reducing the equipment payload as well as increasing the vacant space in rovers for future planetary explorations.

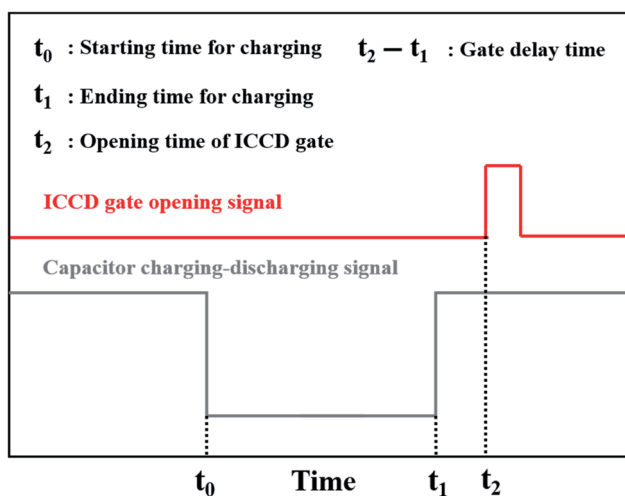


Fig. 2 Time flow chart of the electrical signal for the compact-sized MCU algorithm.

2.2.3 Series of optimization tests for electrode positioning and materials. The following series of experiments was set up to test the significance of each variable concerning the performance of SIBS. Four tests were carried out to determine the most effective setup in optimizing the system. The variables tested include materials, distance, and positioning of the electrode. Four different materials were tested to find their efficiencies in generating electrical sparks, as displayed in Table 3. Those four different materials were chosen for their prevalent usage as electrodes. All the different electrodes were set to a uniform size of 1.0 mm in diameter and length of 7 cm with a 3 mm gap distance. For the varying distance test, a pure tungsten material was used. Two electrodes were separated horizontally with the distance ranging from 1 mm to 5 mm in the electrode gap distance test, while a stand-off distance test was performed to position two electrodes varying vertically from -1 mm to 3 mm with a 3 mm fixed gap distance, as shown in Fig. 3. Trials to vary the angle of electrode pairs on the sample were also performed with different angles to see the differences in signal intensities. Furthermore, an additional stand-off distance test for the aragonite (CaCO_3) pellet sample was enacted to understand the effect of positioning the electrodes.

3. Results and discussion

3.1 Analysis of solid samples using spark-induced breakdown spectroscopy

As stated previously, the main deficiency of using SIBS for detecting bulky materials is the difficulty in the precise positioning of the electrodes. Thus, preceding research was unable to further develop the SIBS method due to this complication.²⁴ However, in Fig. 4, the emission spectrum of each sample was precisely captured, representing a successful optimization of SIBS for bulk samples which will be further discussed in Section 3.3. Regardless of the mechanical difficulty of electrode positioning, the experiment is proved to be successful due to the immense production of a spark. The high-energy spark ensures that a strong plasma is generated which affects the sampling statistics and sensitivity. On the other hand, this high-energy spark can adversely stimulate a high threshold level of plasma

Table 3 Composition information and melting point of four electrode materials used

Material	Composition information	Melting point
Aluminum	Al (99.70%), Si (0.20%), Fe (0.10%)	545–655 °C
Copper	Cu (97.00%), Zn (1.50%), Al (1.25%), Fe (0.20%)	1060–1138 °C
Stainless steel	Fe (65.00%), Cr (15.00%), Ni (3.50%), C (2.00%)	1510 °C
Tungsten	W (99.85%)	3422 °C

continuum that can negatively affect the efficiency of capturing emission signals. Therefore, setting an appropriate gate width and delay time for each sample can decrease the effect of the plasma continuum over the whole spectral range. Despite the proposed solution, Fig. 4 shows the persistent progression of a plasma continuum as a result of the massive production of plasma formation. Due to the large volume of plasma formation, air particles were disintegrated into oxygen, nitrogen, and hydrogen, which are represented as emission lines, despite the absence of those chemicals in the tested samples. The disintegration of the air particles is caused by the weakened dielectric strength as the plasma voltage exceeds the breakdown voltage of the air particles. On that account, emission lines corresponding to the chemical composition of air, namely N II (746.831 nm), O

I (777.417 nm), O II (464.181 nm), and H I (656.285 nm) were ignored. In conjunction with the breakdown of air, Section 3.3 addresses the issue of disintegration of electrode material and its effects on SIBS.

3.2 Comparison of SIBS and LIBS in spectra and calibration curve

To compare the emission spectra of SIBS and LIBS, the samples listed in Table 1 were analyzed. Both methods shown in Fig. 5 were found to be useful for performing solid-phase spectroscopy, with the pulsed energies fixed at 2 J and 50 mJ for SIBS and LIBS, respectively. The signal intensities of SIBS were significantly higher than those of LIBS due to the larger volume of plasma produced.⁴ With the same gate width and delay time of 1

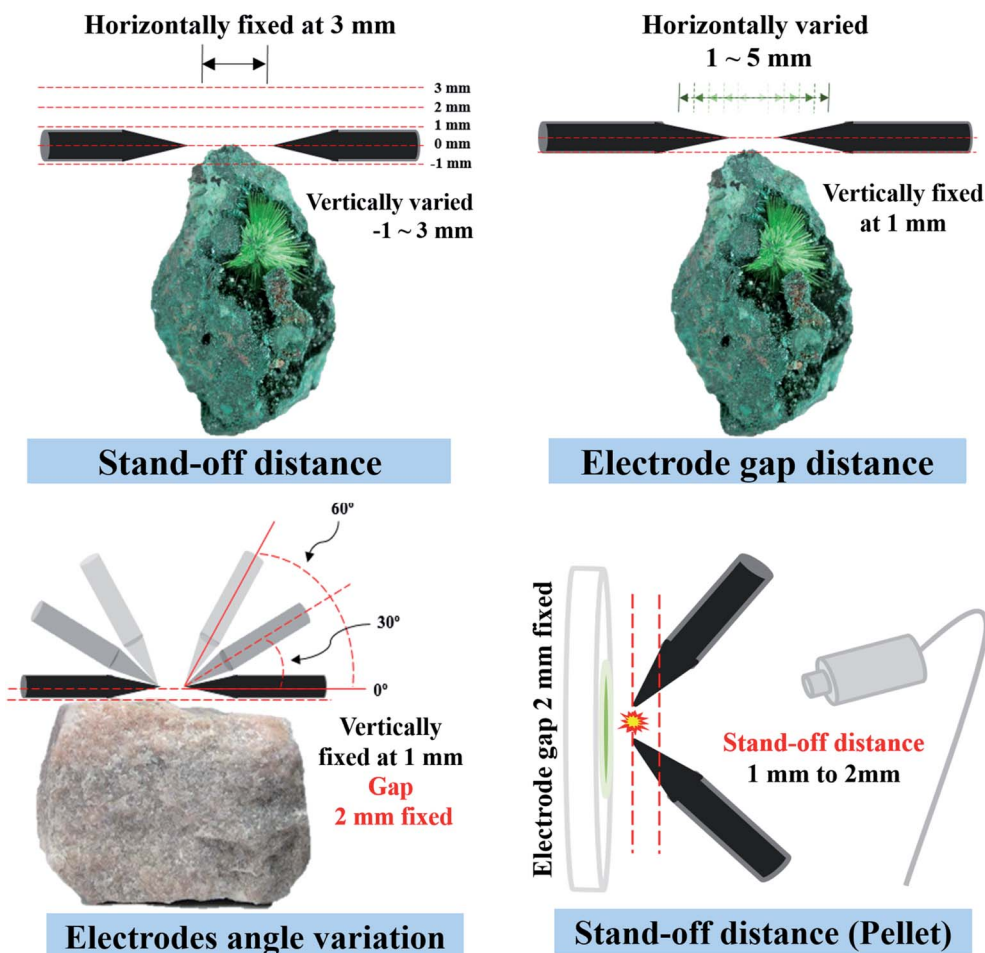


Fig. 3 Schematics of stand-off distance, electrode gap, angle variation, and pellet tests.

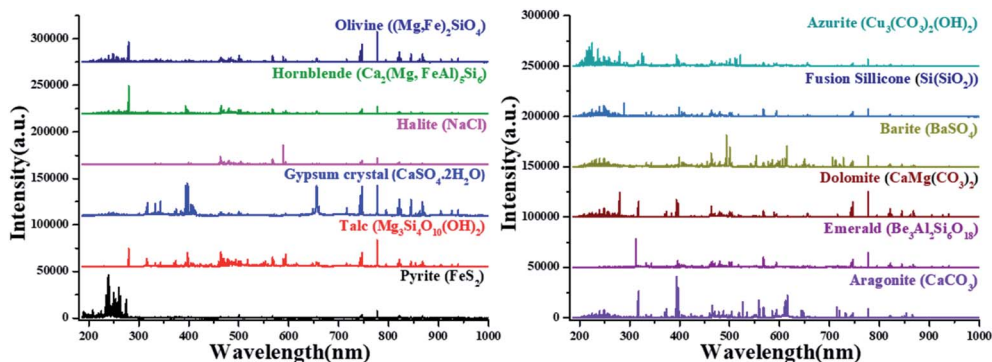


Fig. 4 SIBS emission spectrum of the tested rock samples.

ms and 1 μ s, different plasma continuum results were produced. As a result, the emission lines from SIBS (red colored) are more precise and clearer, while the results from LIBS (navy colored) remained affected by plasma continuum activity. Accordingly, it can be inferred that a spark-induced plasma can excite samples more energetically than laser-induced plasma due to robust plasma production. As shown in Fig. 5, SIBS captured the emission ranges (220 to 400 nm) of metal elements much more easily with higher peak intensities than LIBS. This explains why the SIBS technique was known to be suitable for the bulk analysis of similar samples, for example during steel production in the 1980s as in the spark-OES. It is true that this robust plasma production can lead to some erosion of the sample within a volume of several millimeters, while that of LIBS was in the order of 0.1 mm. For quantitative analysis, the signal-to-noise ratios (SNRs) of both methods were calculated as the ratio of the net atomic emission line intensity to the standard deviation (SD). The SNR of the Ca II (393.366 nm) line in the aragonite sample was set as the index for the calculation. As shown in Fig. 6, the SNR of the Ca II (393.366 nm) line in LIBS was 1.5 times that of SIBS, which implies that the featured emission line is more sensitive in LIBS. This results from the inconsistent performance of using electrodes in SIBS on solid samples rather than the stand-off laser in LIBS. The SNRs for SIBS (54.0777) and LIBS (86.4442) exceed the SNR of 30 which is commonly set as the minimum level for quantitative sampling.

One of the ways to determine the precision of detection is by obtaining the limit of detection (LOD). Prior to analyzing LOD data, signal intensities corresponding to the transition from upper to lower levels of the atomic species need to be identified and can be expressed as eqn (1):

$$I = FN_a^I A_{ul} \frac{g_u}{U_A^I} \exp\left(\frac{-E_u}{K_B T}\right) \quad (1)$$

where I represents the signal intensity, F is the constant instrument parameter for the experimental conditions, N_a^I is the atomic number density, A_{ul} is the transition probability, g_u is the upper-level degeneracy, U_A^I is the partition function for temperature, and E and K are the excited energy and the Boltzmann constant, respectively. The emission intensity, I , of a line is given by eqn (1) assuming the plasma is optically thin and follows the Boltzmann distribution under local

thermodynamic equilibrium (LTE) conditions. Also, with the condition that the temperature and density of each plasma are constant for the same sample and atmospheric conditions, the signal intensity is proportional to the elemental concentration.

The LOD is the lowest quantity of a substance that can be detected and it can be calculated from eqn (2), where σ is the standard deviation of low concentration and S is the slope of the calibration line. In other words, if the LOD from one method is smaller than that from the other, this means the first method can detect more precisely than the other method. A calcite sample was used and the Ca II (393.366 nm) line was chosen to demonstrate the calibration curve in both methods.

$$\text{LOD} = \frac{3\sigma}{S} \quad (2)$$

Fig. 7 compares the calibration curve of calcium (393.366 nm) from SIBS to that from LIBS. As the mass concentration of calcium increased from 1000 to 5000 ppm, the signal intensities also increased accordingly. Table 4 shows that the R^2 values for LIBS are higher than those for SIBS, but it has a lower RSD. This is because of the inconsistent performance of SIBS on solid samples. In addition, it implies that there are fewer plasma variations in laser-induced spectroscopy *versus* spark-induced spectroscopy. Although the R^2 value of SIBS (0.9897) is lower than that of LIBS (0.9931), the slope derived from quantitative SIBS was shown to be 6 times higher than that from LIBSs. The slope value has an inverse relationship with the LOD value, as seen by eqn (2), and the values are 20 and 78 ppm from SIBS and LIBS, respectively. Having a lower LOD value means that it can detect smaller particles. Therefore, SIBS producing such a low LOD has higher sensitivity and accuracy at lower concentration analysis.

3.3 Electrode materials and positioning

The electrodes are important component of SIBS. Four different electrode materials were chosen and stimulated to capture emission signals of pyrite rock samples, as shown in Fig. 8. Apart from those made of tungsten, there was disintegration of materials from the electrodes, which translated

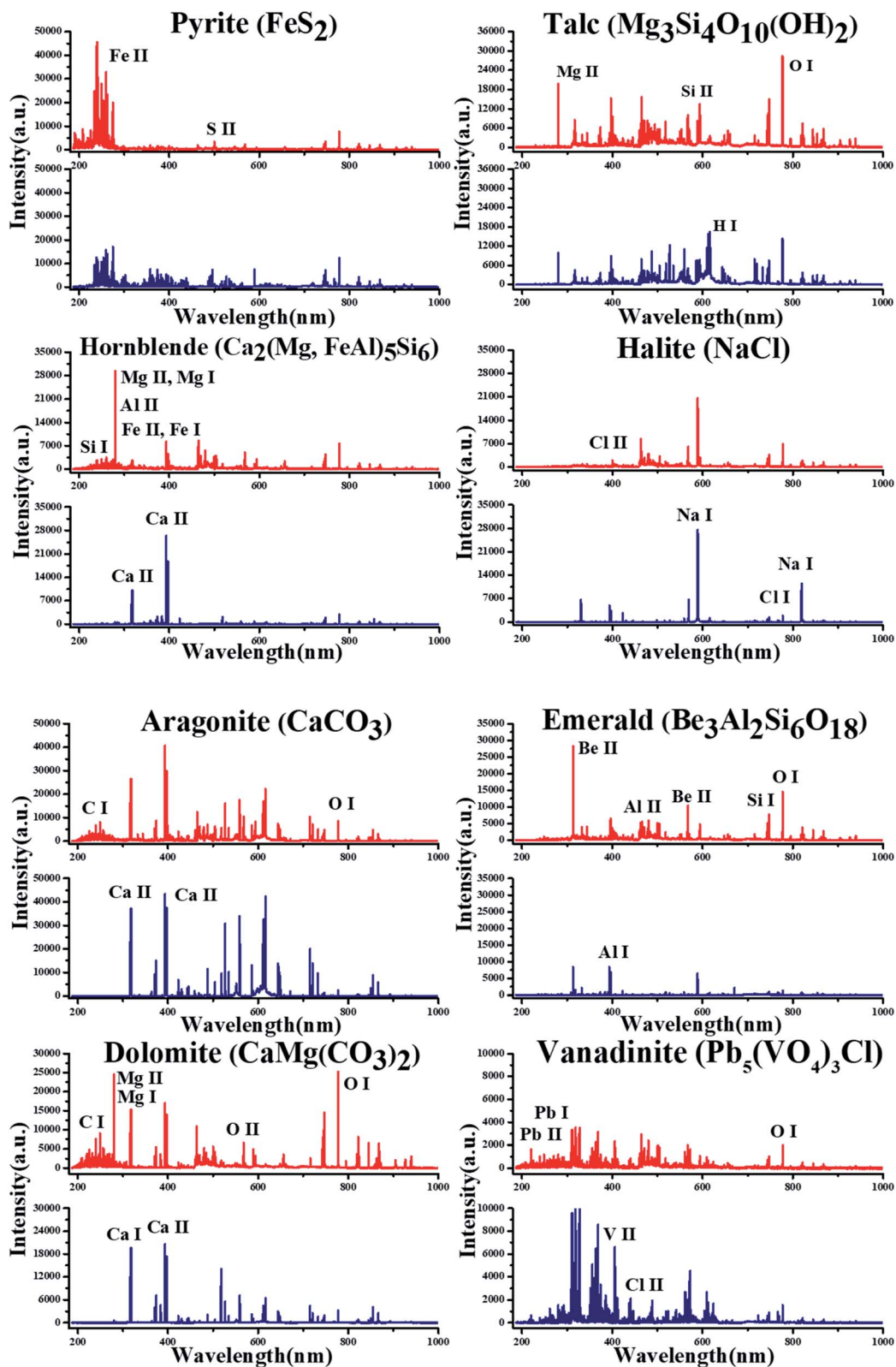


Fig. 5 Emission spectra of the rock samples tested using both methods (SIBS: red coloured, LIBS: navy coloured).

into emission spectrum lines. The disintegration of materials from the electrode appeared as emission line peaks in the emission spectrum. Cu I (324.75, 327.39 nm) appeared from

using copper electrodes and Ni I (341.47, 352.45 nm), and Cr I (357.87 nm) appeared from using stainless steel. These reactions were present due to the corrosion of electrodes in SIBS

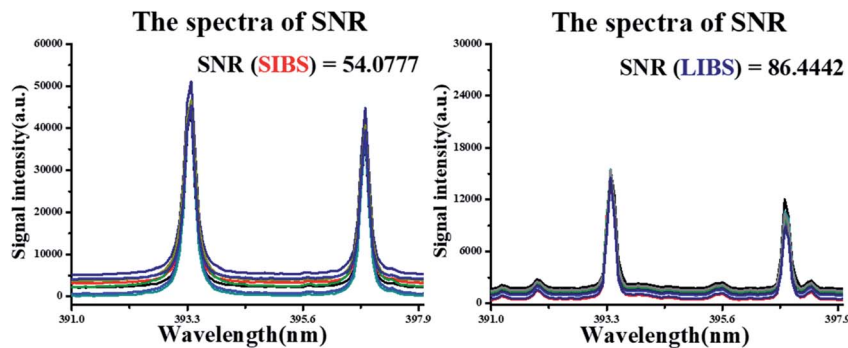


Fig. 6 SIBS and LIBS spectra of SNR at CaCO₃ concentration.

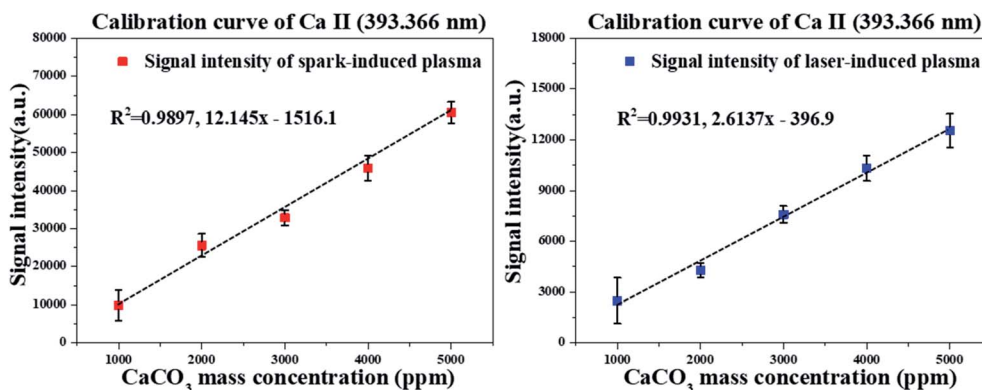


Fig. 7 Ca II (393.366 nm) line calibration curves for SIBS and LIBS.

Table 4 Comparison of SIBS and LIBS for Ca line intensity

Technique	R ² value	RSD (%)	LOD
SIBS	0.9897	2.9869	20 ppm
LIBS	0.9931	1.1568	78 ppm

when a high current was conducted through the electrode. The melting point of each material is listed in Table 3, and they are all prone to material disintegration due to the impact of high heat energy rupturing the plasma. Tungsten, however, overcomes this material disintegration process due to its higher melting point of around 3500 to 4000 °C. In conclusion, the optimum melting point for electrodes to effectively attain SIBS without material disintegration is greater than 4000 °C.

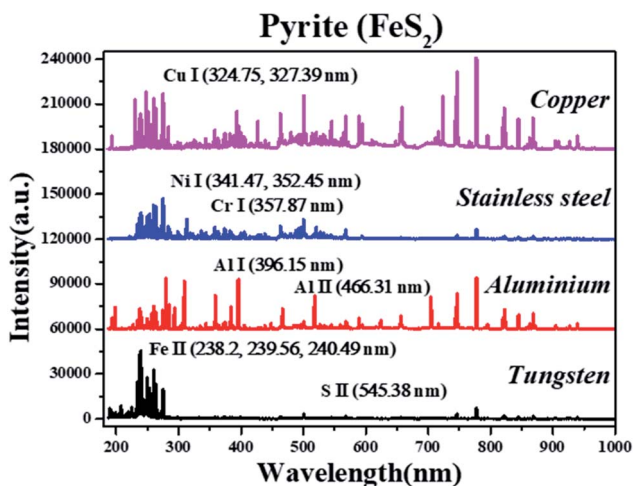


Fig. 8 Plasma emission spectrum of pyrite (FeS₂) sample with four different electrode materials.

It is crucial to maintain the positioning of electrodes around the sample during SIBS because it can significantly skew the signal sensitivity results. Varying the electrode gap can create different types of plasma. A narrow gap creates a small and weak plasma, while wider gaps create an arc plasma which is unable to excite samples to emit an emission spectrum.⁷ Therefore, it is important to find the optimum electrode gap distance for SIBS. As shown in Fig. 9 and 10, setting the electrode gap at 3 mm generates the best signal intensity. Although the results from setting the gap distances at 4 and 5 mm gave higher signal intensities, the rate of success was only 3 out of 30 shots which were not sufficient to contribute to the spectrum data.

Fig. 11 displays the results from the stand-off distance experiment. The outcome showed that setting the stand-off distance vertically at 1 mm from the sample resulted in the highest sensitivity amongst the tested distances. Although the

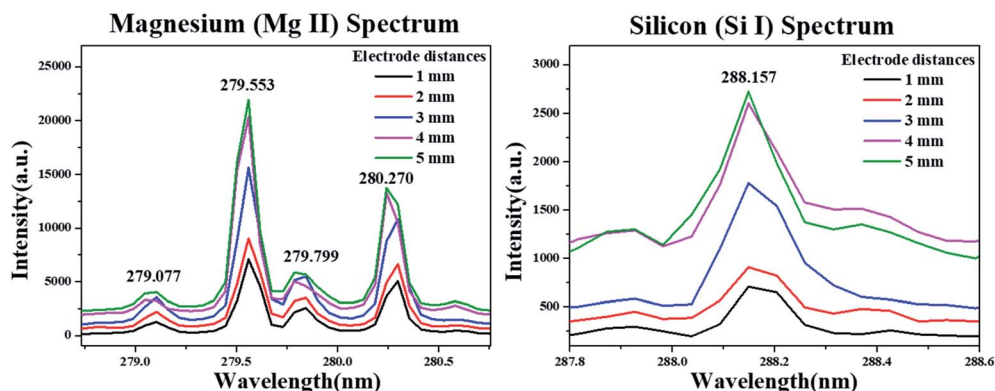


Fig. 9 Electrode gap distances varied (1–5 mm) for olivine ((Mg, Fe)₂SiO₄) rock sample.

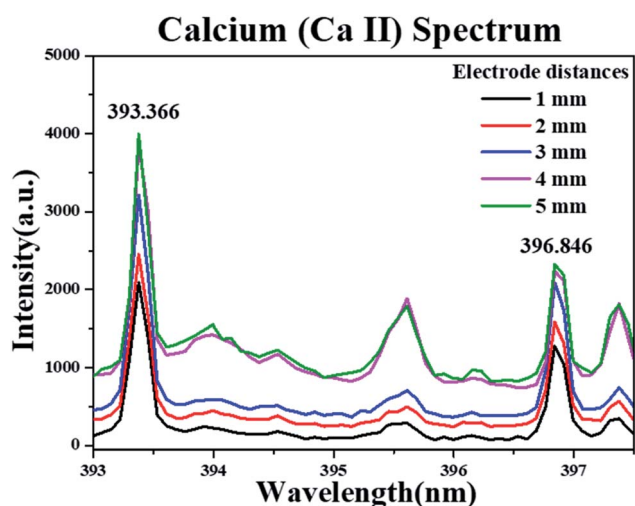


Fig. 10 Electrode gap distances varied (1–5 mm) for aragonite (CaCO₃) rock sample.

results generated from a 0 mm stand-off distance remain important for signal intensities contributing to creating emission line peaks, due to the strong plasma induction and disturbance between the electrode gaps, bringing it into contact

with the samples can cause serious damage to both components in the setup.

Fig. 12 shows a further investigation of the stand-off distance using aragonite (CaCO₃) in pellet form. The significance of this investigation is to compare the trend in results from the bulk sample. The results illustrate that both figures had similar relationships in the ratio between the stand-off distance and signal intensity. When the stand-off distance is set at 1 and 2 mm, both bulk and pellet samples resulted in the same value of signal intensity difference ratio, of around 1 to 15. Thus, confirmed by both methods, setting the stand-off distance vertically at 1 mm results in the highest performance in sensitivities in this setup.

In fact, the spark is generated in the middle, which is the shortest distance between the two electrodes. The spark is generated because the shortest distance between two electrodes acts as the lowest resistance at which the electric field can be produced most strongly. Hypothetically, altering the angle of the electrode should affect the ability to generate a spark since the distance between the electrodes can be changed. However, against all expectations, the angle variation test did not show any significant differences within the range of 0 to 60°, as illustrated in Fig. 13. The reason for this observation was the very thinness of the electrodes. This experiment used narrow-tip

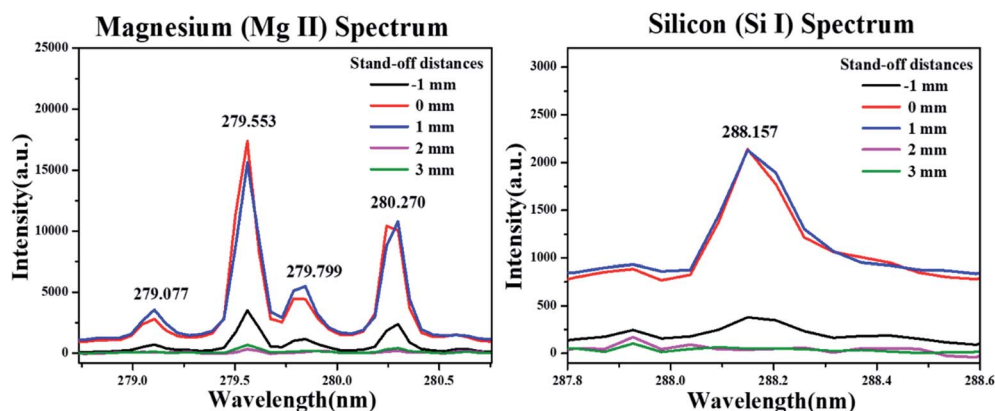


Fig. 11 Electrode stand-off distances varied (–1–3 mm) for olivine ((Mg, Fe)₂SiO₄) rock sample.

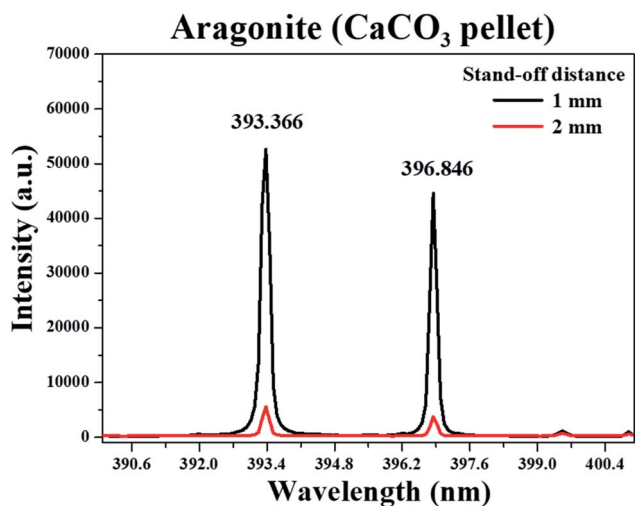


Fig. 12 Electrode stand-off distances varied (1–2 mm) for aragonite (CaCO_3) pellet sample.

electrodes of 1 mm in diameter and 6 cm in length, whose contribution to generating sparks was not affected by the angle variation due to their shape.

3.4 New SIBS for planetary exploration

Laser-induced breakdown spectroscopy is currently in use on board the rover for Mars explorations. *Curiosity* has its *ChemCam* unit as a spectroscopic tool for analyzing the chemical composition of rocks and soil. Due to the advantage of having a longer stand-off distance range, up to 7 meters, the laser-induced spectroscopy method has been widely used. Maurice *et al.*²⁵ analysed the LIBS data collected from *Curiosity* with attributes to interpret *ChemCam* activities and discoveries. They reported that LIBS signals on Mars showed higher signal intensities than instrument surrogates on Earth, due to its lighter pressure of 4.5 Torr which was also thoroughly researched through an LIBS test at low pressure by Choi *et al.*²⁶ In relation to the reported outcome, there is a high possibility of intensity enhancement by SIBS in other environments. As discussed in Section 3.2, SIBS provided a stronger signal with only

a few parts, requiring a simple electrical source input. In addition, signal sensitivities and LOD value were better for SIBS than for LIBS as a result of comparison tests between both methods. The main advantage of LIBS is the use of a stand-off laser pulse. However, due to the level of dust contamination on Mars, this advantage was nullified. Such dust interference and the limitations of camera resolution affected the practical shortening of the *ChemCam* stand-off distance to 4 m, with regard to which, LIBS is still the most optimized and convenient application for remote control rovers. The fact that SIBS was not selected on current space missions may be explained as follows: (i) the electrodes in SIBS must be replaced often due to its self-erosion issues, as discussed in Section 3.3. The SIBS reproducibility is lower with respect to configuration than for LIBS. (ii) SIBS requires closer surface analysis than LIBS, necessitating additional issues of mechanical complexity when packaging. However, if the rover arms attached with SIBS were designed to be extended and had a more accurate movement with stand-off sensors and were equipped with optimal material of electrodes, the implementation of SIBS in collaboration with LIBS as a new approach to spectroscopy would provide a feasible improvement in future space exploration.

4. Conclusion

This work has described the application of SIBS in the real-time detection of constituents of unknown bulk samples. Experimental indices, such as emission line peaks, signal intensity, and LOD, were compared with those of LIBS. The strong energy spark of SIBS generated a larger plasma volume, leading to higher signal intensities, and a better LOD indicated that SIBS is to be preferred for lower concentration samples over LIBS. Also, an optimum SIBS configuration was obtained to decrease its size to a minimum when compared to earlier works in the literature. This is an added advantage of SIBS being mounted on board a rover for planetary missions. Although the low-pressure work was not included as a part of a space mission test, the present work has outlined the detailed optimization scheme and a roadmap for conducting the *in situ* analysis of unknown minerals of a remote environment *via* a compact SIBS unit, potentially mountable on a rover.

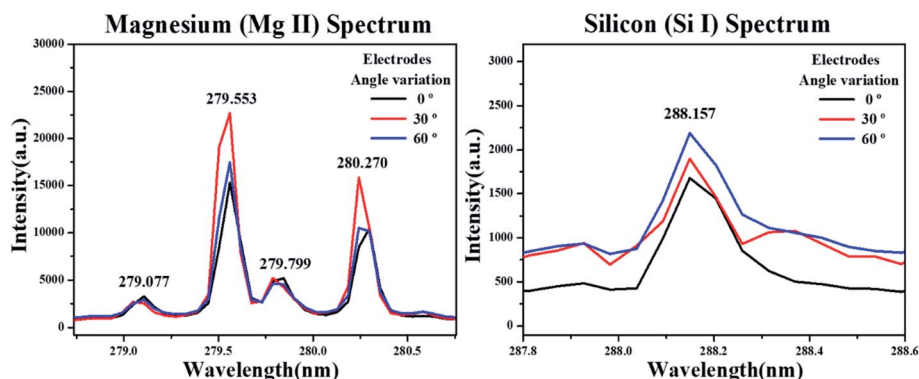


Fig. 13 Electrode angle variation (0–60°) for olivine ($(\text{Mg}, \text{Fe})_2\text{SiO}_4$) rock sample.

Conflicts of interest

There are no conflicts to declare.

Acknowledgements

This work was financially supported by the basic Science Research Program (NRF-2016R1D1A1A02937421) contracted through IAAT and IOER at Seoul National University.

References

- 1 A. W. Miziolek, *Laser-induced Breakdown Spectroscopy (LIBS): Fundamentals and Applications*, Cambridge University Press, Cambridge, 2006.
- 2 *Laser-induced Breakdown Spectroscopy: Theory and Applications*, ed. S. Z. Mussazzi and U. Perini, Springer, 2014, pp. 377–410.
- 3 J. H. Yang, H. M. Jun and J. J. Yoh, Double-pulse laser synchronization aimed at simultaneous detection of enhanced atomic and molecular signals at low pressure conditions, *Spectrochim. Acta, Part B*, 2019, **157**, DOI: 10.1016/j.sab.2019.05.010.
- 4 A. J. R. Hunter, L. G. Piper and A. W. Miziolek, *Spark-induced breakdown spectroscopy: a description of an electrically generated LIBS-like process for elemental analysis of airborne particulates and solid samples*, Cambridge University Press, 2006, pp. 585–614, DOI: 10.1017/cbo9780511541261.019.
- 5 C. Letty, A. Pastore, E. Mastorakos, R. Balachandran and S. Couris, Comparison of electrical and laser spark emission spectroscopy for fuel concentration measurements, *Exp. Therm. Fluid Sci.*, 2010, **34**(3), 338–345, DOI: 10.1016/j.expthermflusci.2009.10.018.
- 6 A. J. R. Hunter, S. J. Davis, L. G. Piper, K. W. Holtzclaw and M. E. Fraser, Spark-induced breakdown spectroscopy: a new technique for monitoring heavy metals, *Appl. Spectrosc.*, 2000, **54**(4), 575–582.
- 7 T. Kammermann, W. Kreutner, M. Trottmann, L. Merotto, P. Solitic and D. Bleiner, Spark-induced breakdown spectroscopy of methane/air and hydrogen-enriched methane/air mixtures at engine relevant conditions, *Spectrochim. Acta, Part B*, 2018, **148**, 152–164, DOI: 10.1016/j.sab.2018.06.013.
- 8 P. K. Srungaram, K. K. Ayyalasomayajula, F. Y. Yueh and J. P. Singh, Comparison of laser induced breakdown spectroscopy and spark induced breakdown spectroscopy for determination of mercury in soils, *Spectrochim. Acta, Part B*, 2013, **87**, 108–113, DOI: 10.1016/j.sab.2013.05.009.
- 9 X. He, B. Chen, Y. Chen, R. Li and F. Wang, Femtosecond laser-ablation spark-induced breakdown spectroscopy and its application to the elemental analysis of aluminum alloys, *J. Anal. At. Spectrom.*, 2018, **12**, DOI: 10.1039/c8ja00261d.
- 10 M. M. Hassanimatin, S. H. Tavassoli, Y. Nosrati and A. Safi, A combination of electrical spark and laser-induced breakdown spectroscopy on a headed sample, *Phys. Plasmas*, 2019, **26**, 033303, DOI: 10.1063/1.5084102.
- 11 D. W. Hahn and N. Omenetto, Laser-induced breakdown spectroscopy (LIBS), part I review of basic diagnostics and plasma-particle interactions: still-challenging issues within the analytical plasma community, *Appl. Spectrosc.*, 2010, **64**, 335A–366A.
- 12 J. Scaffidi, S. M. Angel and D. A. Cremers, Emission enhancement mechanisms in dualpulse LIBS, *Anal. Chem.*, 2006, **78**, 24–32.
- 13 A. M. Popov, F. Colao and R. Fantoni, Spatial confinement of laser-induced plasma to enhance LIBS sensitivity for trace elements determination in soils, *J. Anal. At. Spectrom.*, 2010, **25**, 837–848.
- 14 D. M. Dong, L. Z. Jiao, X. F. Du and C. J. Zhao, Ultrasensitive nanoparticle enhanced laserinduced breakdown spectroscopy using a super-hydrophobic substrate coupled with magnetic confinement, *Chem. Commun.*, 2017, **53**, 4546–4549.
- 15 C. G. de Vega, N. Bordel, R. Pereiro and A. Sanz-Medel, Evaluation of the temporal profiles and the analytical features of a laser ablation-pulsed glow discharge coupling for optical emission spectrometry, *Spectrochim. Acta, Part B*, 2016, **121**, 47–54.
- 16 Y. Wang, Y. Jiang, X. He, Y. Chen and R. Li, Triggered parallel discharge in laser-ablation spark-induced breakdown spectroscopy and studied on its analytical performance for aluminum and brass sample, *Spectrochim. Acta, Part B*, 2018, **150**, DOI: 10.1016/j.sab.2018.10.001.
- 17 P. W. J. M. Boumans, *Theory of Spectrochemical Excitation*, Springer, 1966.
- 18 P. R. Christensen, J. L. Bandfield and V. E. Hamilton, A thermal emission spectral library of rock-forming minerals, *J. Geophys. Res.: Planets*, 2000, **105**(E4), DOI: 10.1029/1998je000624.
- 19 D. C. Catling, On Earth, as it is on Mars?, *Nature*, 2004, **429**, 707–708, DOI: 10.1038/429707a.
- 20 S. Yao, J. Xu, X. Zhang and L. Zhang, Real-time measurement of constituents in solid materials using particle flow spark induced breakdown spectroscopy, *J. Anal. At. Spectrom.*, 2018, **33**, 986, DOI: 10.1039/c8ja00075a.
- 21 N. Taefi, M. Khalaji and S. H. Tavassoli, Determination of elemental composition of cement powder by Spark induced breakdown spectroscopy, *Cem. Concr. Res.*, 2010, **40**, 1114–1119, DOI: 10.1016/j.cemconres.2010.03.003.
- 22 S. Rosenwasser, G. Asimellis, B. Bromley, R. Hazlett, J. Martin, T. Pearce and A. Zigler, Development of a method for automated quantitative analysis of ores using LIBS, *Spectrochim. Acta, Part B*, 2001, **56**, 707–714, DOI: 10.1016/s0584-8547(01)00191-4.
- 23 P. Liu, J. Liu, D. Wu, L. Sun, R. Hai and H. Ding, Study of spark discharge assisted to enhancement of laser-induced breakdown spectroscopic detection for metal materials, *Plasma Chem. Plasma Process.*, 2018, **38**, 803–816, DOI: 10.1007/s11090-018-9900-8.
- 24 A. J. R. Hunter, R. T. Wainner, L. G. Piper and S. J. Davis, Rapid field screening of soils for heavy metals with spark induced breakdown spectroscopy, *Appl. Opt.*, 2003, **42**(12), 2102–2109, DOI: 10.1364/ao.42.002102.

- 25 S. Maurice, S. M. Clegg, R. C. Wiens, O. Gasnault, W. Rapin, O. Forni, A. Cousin, V. Sautter, N. Mangold, L. Le Deit, M. Nachon, R. B. Anderson, N. L. Lanza, C. Fabre, V. Payre, J. Lasue, P. Y. Meslin, R. J. Leveill, B. L. Barraclough, P. Beck, S. C. Bender, G. Berger, J. C. Bridges, N. T. Bridges, G. Dromart, M. D. Dyar, R. Francis, J. Frydenvang, B. Gondet, B. L. Ehlmann, K. E. Herkenhoff, J. R. Johnson, Y. Langevin, M. B. Madsen, N. Melikechi, J. L. Lacour, S. Le Mouelic, E. Lewin, H. E. Newsom, A. M. Ollila, P. Pinet, S. Schroder, J. B. Sirven, R. L. Tokar, M. J. Toplis, C. d'Uston, D. T. Vanimanj and A. R. Vasavadap, ChemCam activities and discoveries during the nominal mission of the Mars science Laboratory in Gale crater, Mars, *J. Anal. At. Spectrom.*, 2016, **31**, 863, DOI: 10.1039/c5ja00417a.
- 26 S. J. Choi and J. J. Yoh, Laser-induced plasma peculiarity at low pressures from the elemental lifetime Perspective, *Opt. Express*, 2011, **19**(23), 23097–23103.